

Noncoincident validation of Aura MLS observations using the Langley Research Center Lagrangian chemistry and transport model

D. B. Considine,¹ M. Natarajan,¹ T. D. Fairlie,¹ G. S. Lingenfelser,² R. B. Pierce,¹
L. Froidevaux,³ and A. Lambert³

Received 10 April 2007; revised 29 August 2007; accepted 31 October 2007; published 29 May 2008.

[1] We evaluate Aura Microwave Limb Sounder version 2.2 measurements of O₃, HCl, and H₂O with version 19 HALOE observations using a model-assisted, noncoincident intercomparison technique. Air parcels in the Langley Research Center Lagrangian chemistry and transport model (LCTM) are initialized from HALOE observations made during three different 3-week periods in 2004 and early 2005. The LCTM tracks the dynamical and photochemical evolution of the ensemble of air parcels following initialization. We show that the LCTM predictions agree closely with subsequent HALOE measurements not used to initialize the model, demonstrating the model's capability to accurately propagate information from the HALOE observations. HALOE-initialized LCTM O₃ predictions agree very well in the stratosphere with MLS measurements, with coincident zonal mean differences generally less than 10%. We find low biases in HCl of 10–30% relative to the MLS observations. We also find low biases with respect to MLS H₂O of up to 15% in the upper and middle stratosphere and ~30% low biases in the lower stratosphere/upper troposphere midlatitudes. We note some nonphysical vertical oscillations of MLS H₂O in the tropical and midlatitude lower stratosphere that are not present in the HALOE-initialized LCTM output. The oscillations are smaller in version 2.2 than in previous versions. These results are generally consistent with published HALOE/MLS intercomparisons of these species using a traditional coincident validation technique. This consistency suggests that the traditional coincident validation results are applicable on daily temporal and zonal spatial scales.

Citation: Considine, D. B., M. Natarajan, T. D. Fairlie, G. S. Lingenfelser, R. B. Pierce, L. Froidevaux, and A. Lambert (2008), Noncoincident validation of Aura MLS observations using the Langley Research Center Lagrangian chemistry and transport model, *J. Geophys. Res.*, 113, D16S33, doi:10.1029/2007JD008770.

1. Introduction

[2] The NASA Aura satellite was launched on 15 July 2004, into a sun-synchronous, 705 km altitude orbit, with a 98.2° inclination. The instruments on board the satellite began taking data a few weeks after the launch. The satellite carries 4 instruments: the Microwave Limb Sounder (MLS), the Tropospheric Emission Spectrometer (TES), the Ozone Monitoring Instrument (OMI), and the High-Resolution Dynamics Limb Sounder (HIRDLS). Together, these instruments are providing a large number of atmospheric composition measurements, which will add substantially to the database of observations of the mesosphere, stratosphere, and troposphere. To be useful, these measurements must be quantitatively compared to existing, well-understood measurements of atmospheric composition for consistency and

quality. This paper evaluates measurements of O₃, H₂O, and HCl made by the MLS instrument.

[3] The primary method of evaluating differences between observations of some physicochemical quantity from two different instruments is by comparing observations made concurrently, in the same geophysical location. Such coincidences are relatively rare, especially if one or both of the instruments use a sparse sampling technique such as solar occultation. For instance, *Froidevaux et al.* [2006] compared occultation observations of O₃, H₂O, and HCl made by the Halogen Occultation Instrument (HALOE) on board the Upper Atmosphere Research Satellite (UARS) with Aura MLS measurements using a traditional coincident approach. With their coincidence criteria of within 1° latitude, 12° longitude, and 6 h, they found ~300 coincident profiles between January and March of 2005, ranging from 75°S to 52°N.

[4] A second method is the so-called “noncoincident” intercomparison. In this technique, a model of some type is used to connect measurements from the two instruments that were made at different locations and/or times [e.g., *Lait et al.*, 2004; *Morris et al.*, 2002; *Danilin et al.*, 2002]. Opportunities for comparison increase substantially because this method relaxes the need to sample the same air mass at

¹NASA Langley Research Center, Hampton, Virginia, USA.

²Science Systems and Applications International, Inc., Hampton, Virginia, USA.

³Jet Propulsion Laboratory, California Institute of Technology, Pasadena, California, USA.

the same time. The disadvantage of this technique is that it introduces additional sources of uncertainty into the comparison due to the use of a model.

[5] The Langley Research Center Lagrangian chemistry and transport model (LCTM) [Pierce *et al.*, 2003] can be used for noncoincident intercomparison of observations. The LCTM calculates the dynamical and photochemical evolution of an ensemble of air parcels that have been initialized at the locations of atmospheric composition observations made by satellite, balloon, or aircraft platforms. When these parcels are later observed by a second instrument, the parcel composition as predicted by the LCTM can be compared to the observations. Provided the LCTM prediction is strongly influenced by the initial observations and the air parcels are still relatively well-defined, comparison of the LCTM predictions with the second instrument will test the consistency of the observations made by the two instruments.

[6] In this paper we use the LCTM to compare Aura MLS observations of O₃, HCl, and H₂O with occultation observations made by the HALOE instrument. HALOE operated on the Upper Atmosphere Research Satellite (UARS) between 12 September 1991 and 21 November 2005. Data from the HALOE instrument have been examined extensively and are very well established. We focus on three periods during the July 2004 to November 2005 overlap period. The periods were selected because there were sufficient HALOE observations to initialize the LCTM (at least 14 d of observations during the period), and version 2.2 MLS observations for comparison were available at the end of the periods. These periods are as follows: 27 August to 17 September 2004, 8–29 November 2004, and 18 January to 8 February 2005. Currently these are the only three periods satisfying these criteria during the HALOE/Aura MLS overlap period. Note that the version 2.2 MLS data has two variants: a version 2.20 and version 2.21, which includes a very minor software fix that is not in version 2.20. Since our results apply to either version, we refer to both variants as version 2.2 data for the remainder of this paper.

[7] It should be noted that the intercomparison of measurements made by two different instruments can only determine the consistency of the measurements. It does not indicate which, if either, of the measurements is correct. However, if significant differences are found, there would be a need to understand and reconcile those differences. Thus, measurement intercomparison is an important first step in instrument validation.

[8] In section 2 we discuss relevant characteristics of the HALOE data. Section 3 provides a model description, including our method for calculating overhead column ozone. Section 4 sketches the LCTM runs we conducted, and section 5 evaluates the capability of the LCTM to propagate HALOE information via a comparison with HALOE measurements. Sections 6 and 7 present the results of our comparisons with MLS observations. A summary and some conclusions are discussed in section 8.

2. HALOE Data

[9] The HALOE instrument is a multichannel broadband radiometer. It flew on board the Upper Atmosphere Research Satellite (UARS), which was in a 57° inclination

orbit at an altitude of 585 km. The instrument used infrared solar occultation, acquiring profile data during ∼15 sunrise and ∼15 sunset events each day. The latitude ranges of these measurements varied over the course of the year. Figure 1 shows the latitudes of the HALOE profiles acquired during August/September 2004, November 2004, and January/February 2005, as a function of Julian day. Vertical dashed lines bound the time periods simulated in this paper.

[10] HALOE O₃ observations were made with the 9.6 micron channel [Russell *et al.*, 1993]. The vertical resolution of the measurement is ∼2 km. Version 17 error estimates range from ∼11% at 0.1 hPa, with the error evenly split between random and systematic sources, to ∼30% at 100 hPa, with the error at this pressure mostly systematic [Brühl *et al.*, 1996]. HALOE CH₄ was measured using a gas filter correlation technique using the instrument's 3.3 micron channel [Park *et al.*, 1996]. All HALOE gas filter correlation measurements are retrieved with a ∼4 km vertical resolution. The estimated error of the measurement ranges from ∼6% in the upper stratosphere to about 20% near 100 hPa, so it has the lowest estimated error of any of the HALOE species discussed in this paper. HALOE used the same channel to measure HCl, again using a gas filter correlation technique to deal with strong interference from the CH₄ signal. Error estimates range from ∼15% at 1 hPa to ∼24% at 100 hPa [Russell *et al.*, 1996]. The HALOE water vapor measurement was made using the 6.6 micron channel of the radiometer. No gas filter was used for this measurement, so effective vertical resolution is ∼2 km. Root-sum-squared error estimates are ∼15% in the 1–5 hPa region, increasing to ∼20% in the upper stratosphere and ∼27% near 100 hPa. Random error dominates in the upper stratosphere, while systematic error dominates in the lower stratosphere error estimates [Harries *et al.*, 1996].

3. Model Description

[11] The Langley Research Center LCTM uses observations of ozone and other key species to initialize an evolving ensemble of air parcel trajectories, and then predicts subsequent photochemical, microphysical, and diffusive tendencies along these trajectories. In previous applications the model has been initialized with occultation observations from several satellite instruments (HALOE, POAM III, SAGE II) and its predictions compared to aircraft data from field missions (ASHOE/MAESA, POLARIS, SOLVE, SOLVE II), as well as balloon data [Pierce *et al.*, 1999, 2003]. In this section we focus on details that have been changed from previous versions.

[12] For this study the model is driven by 3-d meteorological data from the NASA Global Modeling and Assimilation Office (GMAO) version 4 data assimilation system (GEOS-4 DAS) [Bloom *et al.*, 2005]. The meteorological data were generated by the “late-look” DAS, which is generated after the “first-look” analysis and assimilates more observations. The LCTM uses GEOS 4 DAS-generated surface pressure, horizontal wind fields, vertical pressure velocity, and temperature. Each of these fields are provided as 6-h averages, 4 times per day (0000 UT, 0600 UT, 1200 UT, and 1800 UT). The gridded fields have a 1.25° longitude by 1° latitude resolution, and the 3D fields

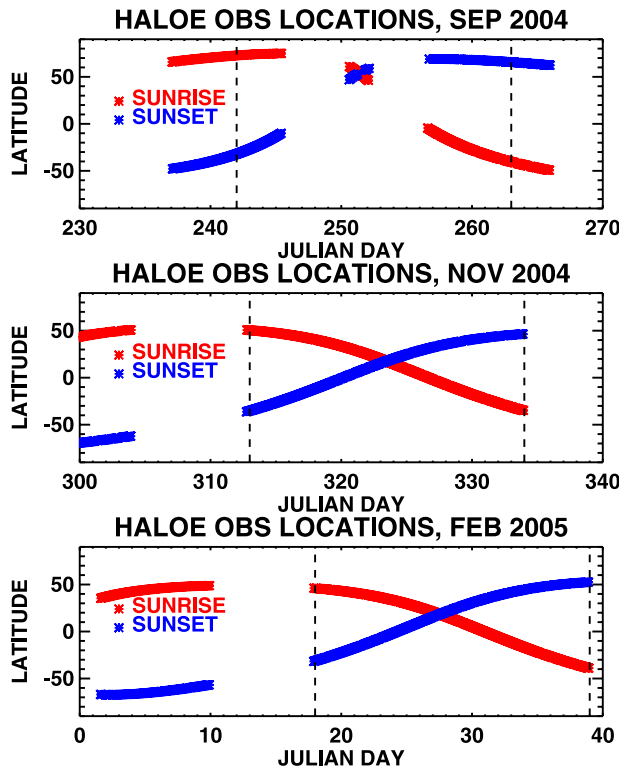


Figure 1. Latitude locations of HALOE occultation observations made during three 40-d periods around September 2004, November 2004, and February 2005. Sunrise locations are marked by a red asterisk; sunset locations are marked by a blue asterisk. Vertical lines show the boundaries of the periods simulated by the LCTM.

are specified at 55 levels in a hybrid sigma-pressure coordinate system. The top edge of the highest layer is at 0.01 hPa. The vertical levels are isobaric from the grid top to the 42nd level (top down numbering), which has a lower edge pressure of 176.93 hPa. The remaining vertical levels are sigma coordinates.

[13] Given the geographic location at a time t of an air parcel being tracked by the LCTM at longitude x_i , latitude y_i , and pressure p_i , the LCTM interpolates from the meteorological data to obtain the horizontal winds u_i , v_i , and vertical pressure velocity ω_i at the parcel location. The model then uses a fourth-order Runge-Kutta advection method with a twenty minute time step to predict an updated parcel location. It is worth noting that this purely kinematic approach using a vertical pressure velocity differs from previous versions of the LCTM, where the vertical coordinate was potential temperature, and the model used diabatic heating rates from a radiative heating calculation. (This change was motivated by a desire to eliminate dependence on a climatological description of the tropospheric temperature distribution and improve UT/LS transport.)

[14] The model diffusive mixing parameterization is described by *Fairlie et al.* [1999] and *Pierce et al.* [2003]. Neighboring parcels are subjected to a background mixing with a relatively weak 60-d timescale, supplemented by rapid mixing ($\sim 1\text{--}2$ d timescale) in regions with a high mixing efficiency factor, a quantitative measure of the

importance of strain relative to rotation on fluid elements in an Eulerian reference frame.

[15] Heterogeneous chemical reactions occur on background sulfate aerosol particles and on parameterizations of both Type 1 (NAT) and Type 2 (ice) polar stratospheric clouds, as is detailed by *Pierce et al.* [2003]. PSC sedimentation vertically redistributes NO_y and H_2O between trajectories. Type 1 PSC sedimentation assumes particle diameters of $\sim 1\text{--}2$ microns, while Type 2 PSC sedimentation assumes particle diameters of ~ 20 microns. Note that these assumptions are not consistent with the observed presence of large Type 1 PSCs, which can fall rapidly and produce denitrification without dehydration [*Fahey et al.*, 2001].

[16] LCTM air parcels were initialized using version 19 HALOE observations as presented by *Pierce et al.* [2003]. The HALOE measurements used for initialization were: NO, NO_2 , H_2O , O_3 , HCl , CH_4 , HF, and aerosol surface area density. The measurements were first interpolated to a set of 21 potential temperature surfaces between 360 K and 2000 K, to allow generation of the set of auxiliary data (chemical species, etc.) that the LCTM requires for initialization. At each potential temperature surface, the auxiliary variables were obtained from HALOE CH_4 and sunrise or sunset mappings between CH_4 and each auxiliary variable. The species- CH_4 - θ maps were generated using output from the LaRC IMPACT GCM [*Al-Saadi et al.*, 2004], as described by *Pierce et al.* [2003]. All model chemical reaction rates and photolysis cross sections have been updated to the *Sander et al.* [2006] recommendations.

[17] Overhead column ozone is required to calculate photolysis rates for use in the model photochemical calculations. To generate these distributions, we used a PV-mapping technique and daily Aura v1.51 MLS level 2 ozone distributions. (We use v1.51 data to construct the overhead column ozone because v2.2 data is not continuously available throughout the time periods we examine.) The version 1.51 MLS data were filtered by the recommended status, quality, and precision values (only values with zero Status flag, Quality flag greater than 0.1, and a positive precision [*Livesey et al.*, 2005]). We used ozone values between 400 and 0.1 hPa, a range slightly larger than the suggested range of 215 to 0.46 hPa. (Retrievals at altitudes below 215 hPa are basically the a priori climatology. Their use will not affect stratospheric overhead column ozone calculations.) GEOS 4 DAS meteorological fields of potential vorticity (PV) and potential temperature (θ) for that day are then interpolated to the locations, pressures, and times of the ozone data using GEOS 4 DAS pressure fields.

[18] The MLS ozone data are then binned by θ and PV. PV bins are logarithmically spaced, and Northern and Southern Hemisphere values are binned separately. We attempt to filter out obvious cloud contamination by excluding ozone values greater than 0.1 ppmv at θ values less than 350 K and PV less than 1 potential vorticity unit (PVU). Locations characterized by these potential temperature and vorticity values are certainly in the troposphere, where O_3 values rarely exceed 0.1 ppmv. The ozone values in each PV- θ bin are averaged together. Bins without ozone data are filled using a cubic spline interpolation in PV. The resulting PV- θ ozone maps are then used along with the 3d fields of PV and θ to generate a 3d ozone distribution at the

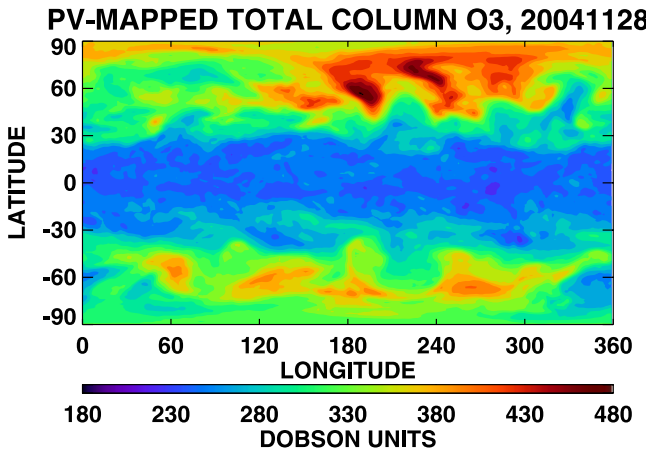


Figure 2. Column O₃ distribution at 0000 UT on 28 November 2004, obtained by potential vorticity mapping technique, as described in the text, using potential vorticity from GEOS 4 DAS meteorological data and MLS v.1.51 O₃ data.

same geographic and temporal resolution as the meteorological data. Constructing overhead column ozone from this distribution is straightforward.

[19] Figure 2 shows an example of the total ozone distribution generated using this method, for 28 November 2004. The high-resolution total ozone field appears to be realistic, with tropical values of $\sim 230\text{--}250$ DU and mid-latitude values of $\sim 300\text{--}450$ DU. To evaluate the quality of these PV-mapped total ozone distributions and the high-resolution, gridded ozone fields that were used to generate them, we compared them to Aura MLS observations made on the same day. (At a minimum we should be able to recover the MLS O₃ values from the high-resolution distributions. However, such a comparison will not reveal if the MLS O₃ data are in error.) The PV-mapped ozone and overhead column ozone distributions were interpolated to the locations and times of the MLS profiles; we then calculated root-mean-square (rms) deviations between the MLS profiles and the PV-mapped profiles in 10° latitude bands from pole to pole. (We calculate the RMS deviation at a particular latitude bin and pressure level from the set of differences $\{d_i\}$, $i = 1, \dots, N$ between the N MLS observations and their corresponding interpolated PV-mapped ozone values at that location. The RMS deviation is taken to be $R = \sqrt{\langle d^2 \rangle}$, where the brackets denote an average over the N values.)

[20] Figure 3a shows as a function of latitude and pressure the RMS deviation between PV-mapped and MLS O₃ profiles, and Figure 3b shows the RMS deviation between PV-mapped and MLS column O₃. The RMS deviation of profile ozone is $\sim 10\%$ throughout most of the stratosphere. It increases to $\sim 30\%$ near the top of the stratosphere. Relatively large values of up to 100% occur in the tropical lower stratosphere, below ~ 100 hPa. This may be due to the cloud-clearing filter mentioned above. There are also relatively high RMS values of $\sim 50\%$ in the SH high latitudes, where the variance of O₃ in a particular PV-θ bin may be large because of small-scale ozone depletion, nonuniform recovery, or incomplete mixing of depleted and

background air. Figure 3b shows the overhead column O₃ RMS difference. Agreement of the PV-mapped and MLS column O₃ is excellent throughout the lower and middle stratosphere, with RMS differences between 5 and 10%. In the upper stratosphere RMS differences increase to $\sim 50\%$. Because noncoincident validation is most useful in the lower to middle stratosphere because of the relatively long lifetimes at these altitudes of the species being examined (O₃, H₂O, and HCl), Figure 3 indicates that the PV-mapped column ozone distributions we have generated can be used in model photolysis calculations due to the low lower to middle stratosphere RMS differences.

4. Run Description

[21] Figure 1 shows the locations of the HALOE observations made during the three periods considered in this paper. Vertical dashed lines bound the simulation periods. During the 27 August to 17 September period (Figure 1, top), HALOE observations were made on 14 d. There is a gap without observations in the NH tropics through lower NH midlatitudes. During the 8–29 November period, 21 d

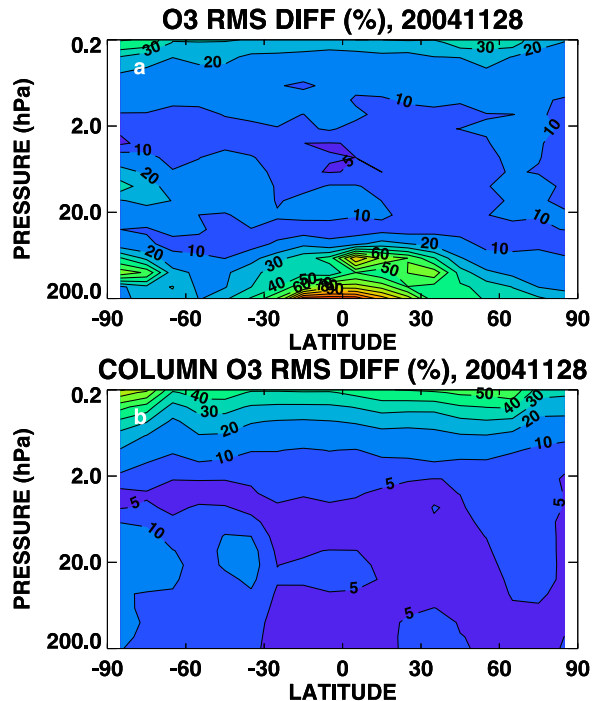


Figure 3. (top) Root-mean-square difference, in percent, between MLS v1.51 O₃ data and PV-mapped profile O₃, at 0000 UT on 28 November 2004. The RMS difference was calculated by binning the MLS observations and their corresponding interpolated PV-mapped ozone values at each Aura pressure level into 10° latitude bins. The RMS difference at a location is given by $R = \sqrt{\langle d^2 \rangle}$, where the brackets denote an average and d represents the set of differences $\{d_i\}$ at that location. The RMS difference is expressed as a percent of the mean of the MLS values at each location. (bottom) Root-mean-square difference between the overhead O₃ column calculated from MLS v1.51 O₃ data and the overhead O₃ column calculated from PV-mapped profile O₃.

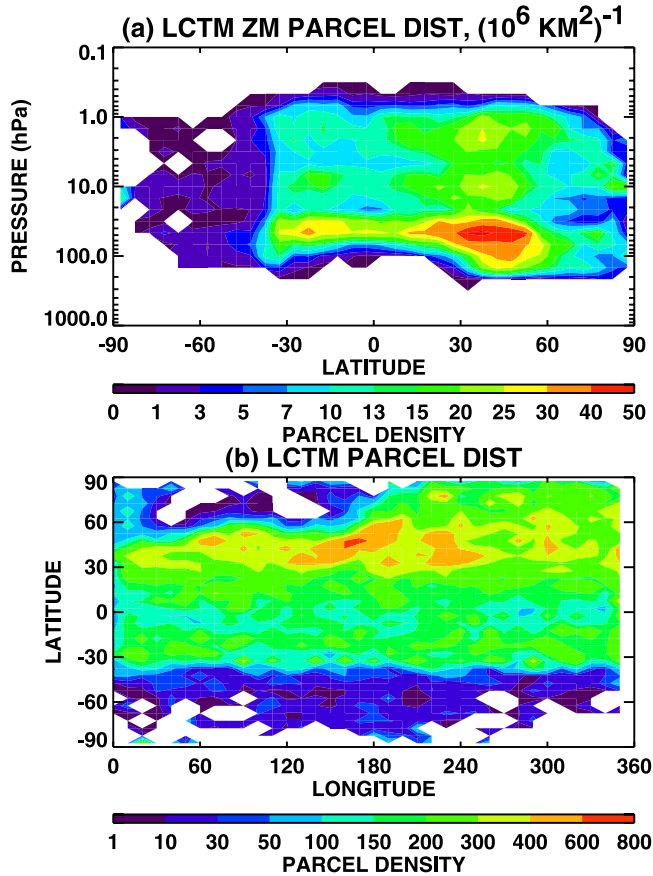


Figure 4. LCTM geographic parcel density distributions on 29 November 2004. Units are number of parcels per million square kilometers. Horizontal resolution is 5° longitude by 4° latitude. (a) Zonal mean parcel distribution, expressed as parcels per 10^6 km^2 in the grid box centered on each of the standard six-level-per-decade Aura pressure levels (a “partial column” unit). (b) Vertically integrated, or “column” parcel distribution. Note the substantially lower parcel densities south of approximately -40°S and in the NH polar vortex region north of $\sim 50^\circ\text{N}$ in the Eastern Hemisphere.

of HALOE observations extend from $\sim 40^\circ\text{S}$ to $\sim 50^\circ\text{N}$, with more NH than SH observations (Figure 1, middle). The distribution of observations during the 18 January to 8 February time period is similar to November. During these time periods, LCTM parcels were initialized from HALOE observations only when the estimated errors for the HALOE species were all less than 30%. Ten LCTM parcels were initialized along the HALOE tangent path of each measurement, equally distributed along a 300 km distance surrounding the tangent altitude location. Once initialized, parcels were transported kinematically using the analyzed horizontal wind and vertical pressure velocities. Parcel trajectories were followed for a maximum of 21 d, after which they were removed from the ensemble. (After 21 d, a typical lower stratospheric, NH midlatitude cluster of parcels initialized from the same measurement has spread in latitude by $\sim 10\text{--}15^\circ$, in longitude by $\sim 40\text{--}50^\circ$, and in altitude by ~ 1 km. We judged parcels older than this to be too ill defined to be useful.) Parcel locations as well as the values

of all model constituents were recorded every 6 h, at 0000 UT, 0600 UT, 1200 UT, and 1800 UT. A total of 61,340 parcels were initialized in the first simulation period by 17 September, 87,080 in the second period by 29 November, and 86,660 by 8 February in the third. As an example, the zonal mean and vertically integrated parcel density distributions on 29 November are shown in Figures 4a and 4b. Figure 4 shows that the highest parcel densities extend from $\sim 30^\circ\text{S}$ to $\sim 60^\circ\text{N}$, with a very rapid decrease at higher latitudes in the SH and a more gradual decrease poleward of $\sim 60^\circ\text{N}$. Figure 4b shows that very few parcels have entered the region of the NH polar vortex, which is located north of $\sim 55^\circ\text{N}$ in the Eastern Hemisphere. The higher concentration of parcels in the lower stratosphere shown in Figure 4a results from the relatively narrow spacing of the theta surfaces on which parcels are initialized in the lower stratosphere. The narrow spacing in the lower stratosphere better preserves any lower stratospheric vertical structure that might occur in the HALOE data initializing the LCTM.

5. Comparison to HALOE Observations

[22] Since the LCTM is initialized with HALOE observations, its ability to transfer information from those HALOE observations forward in time can be tested by comparing model predictions with subsequent HALOE observations. We therefore compare LCTM predictions with HALOE observations made on 28 November 2004, the last day of HALOE observations for the month.

[23] For each of the occultation observations made by HALOE on 28 November 2004, we searched through and identified the set of LCTM parcels satisfying the coincidence criteria of 10° of longitude and 2° of latitude, on the same day as the HALOE observations. These values were chosen on the basis of sensitivity studies of the effect of different criteria on the comparisons. The comparisons were not very sensitive to the time or longitude windows, but were more sensitive to latitude. The chosen criteria are conservative, and each could be relaxed by a factor of two without significantly affecting the results. We also used a vertical pressure grid with the same resolution as the HALOE pressure levels. Note that this resolution in pressure generally exceeds the actual 2–4 km resolution of the HALOE observations. However, we chose to use the reported vertical resolution rather than degrade the vertical resolution of the HALOE observations prior to comparison with LCTM results. Only parcels older than 3 h were considered to prevent comparison of a HALOE observation with the parcels initialized by that same HALOE observation. If more than one parcel satisfied the coincidence criteria, parcel values were averaged together to produce a coincident LCTM prediction. If no LCTM parcels satisfied the coincidence criteria, the HALOE occultation was excluded from the data set. The result of this process is a set of HALOE measurements made on 28 November, with a coincident LCTM prediction for each HALOE measurement.

[24] Figure 5 shows scatterplots of the coincident LCTM predictions (obtained by applying the coincidence criteria described above) against their corresponding HALOE measurements for O₃, CH₄, HCl, and H₂O. Each point on these plots represents one HALOE measurement and its

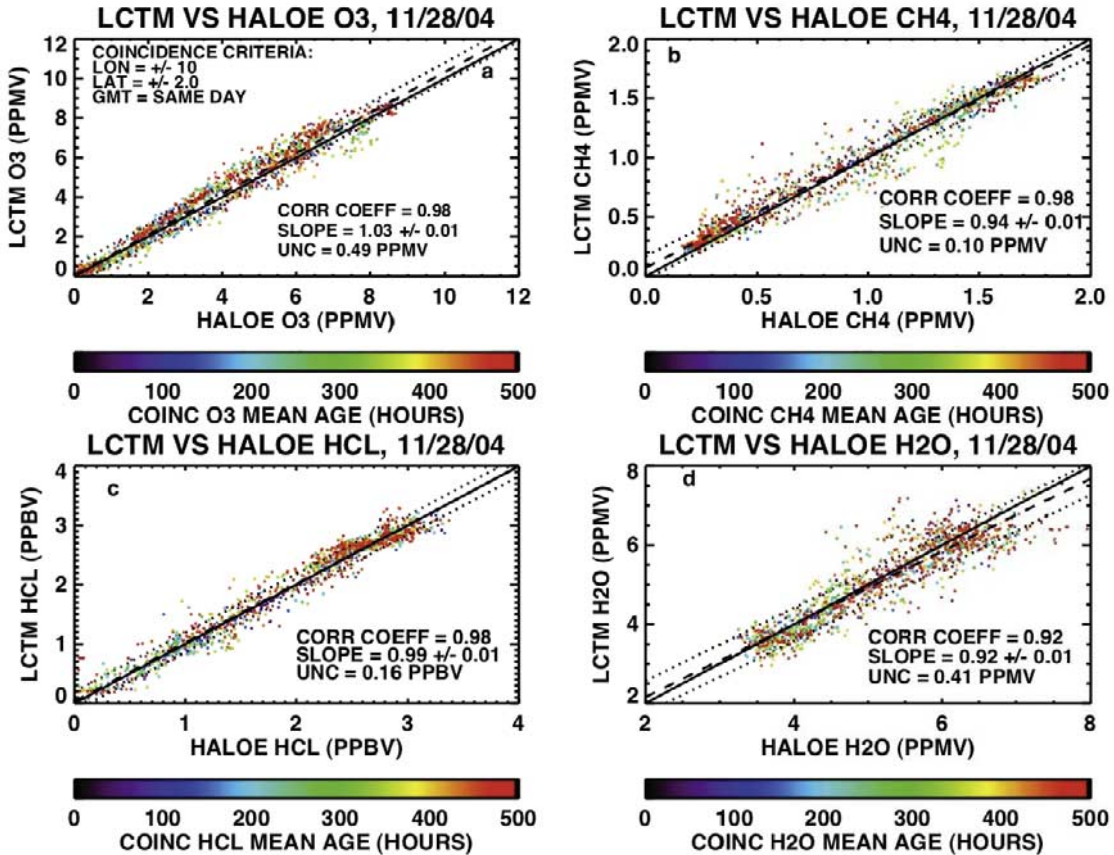


Figure 5. Correlation scatterplots of LCTM: (a) O₃, (b) CH₄, (c) HCl, and (d) H₂O coincident with HALOE observations on 28 November 2004. Coincident LCTM values are color-coded by mean age of the coincident parcels. Solid line shows 1:1 slope. Dashed line shows linear regression fit. Dotted lines show $\pm 1\sigma$ uncertainty around best fit line.

corresponding LCTM prediction. The points are colored by the mean age of the coincident parcels averaged together to produce the LCTM value. Figure 5 shows very good to excellent agreement for O₃, CH₄, and HCl, with slopes close to unity, slope errors of $\sim 1\%$, and linear correlation coefficients of 0.98. Figure 5d shows a slight low bias for H₂O at higher values, and a weaker correlation of 0.92. Note that the correlations themselves should not be over-interpreted, because they depend not only on the uncertainty of the individual LCTM predictions, but also the range of observational values of each species included in the plot. For instance, the ratio between the range of O₃ values (10 ppmv) to the LCTM prediction uncertainty (0.49 ppmv, see Figure 5) is ~ 20 . Figure 5d shows the range for H₂O to be $\sim 4\text{--}5$ ppmv, with a ~ 0.4 ppmv uncertainty, a ratio of ~ 10 . The correlation coefficient is correspondingly smaller, even though the uncertainty for H₂O is actually a little less than it is for O₃. Similarly, if we made correlation plots using subsets of the data which restrict the range of the observation values, the correlation coefficients would be correspondingly smaller.

[25] The O₃ scatterplot (Figure 5a) reveals a slight model high bias for HALOE observations in the 8–9 ppmv range. Figure 5b shows the tightest correlations for CH₄ at the lowest and highest values, with a looser correlation in between. This may be due to the fact that the largest

meridional gradients of CH₄ occur in this range of CH₄ values ($\sim 0.75\text{--}1.25$ ppmv). Figure 5 shows relatively little dependence of the scatter in LCTM values on parcel age, suggesting that the 3-week parcel age limit is sufficient for this comparison.

[26] To understand in more detail how well LCTM results compare with subsequent HALOE measurements, Figure 6 compares NH and SH average HALOE O₃ profiles with LCTM profiles generated using coincident LCTM predictions. HALOE observations on a particular day are made at nearly the same latitude. Figure 1 (middle) shows that HALOE sunset observations on 28 November were made at $\sim 45^\circ\text{N}$, while sunrise observations were located at $\sim 35^\circ\text{S}$. The profiles shown in Figure 6 approximate zonal mean profiles at 45°N and 35°S in the NH and SH, respectively. Figure 6a shows excellent agreement between the LCTM and HALOE profiles in the NH up to ~ 5 hPa, with a small high bias above this value. Figure 6a also shows profiles generated from a passive advection run of the LCTM, including neither chemical nor diffusion operators (black lines). The passive advection case closely matches the full LCTM run up to $\sim 10\text{--}20$ hPa. At higher altitudes the active and passive LCTM runs sandwich the HALOE observations, showing that the effect of chemistry on O₃ at higher altitudes is substantial. Figure 6a also plots the standard deviations of the HALOE and LCTM profiles,

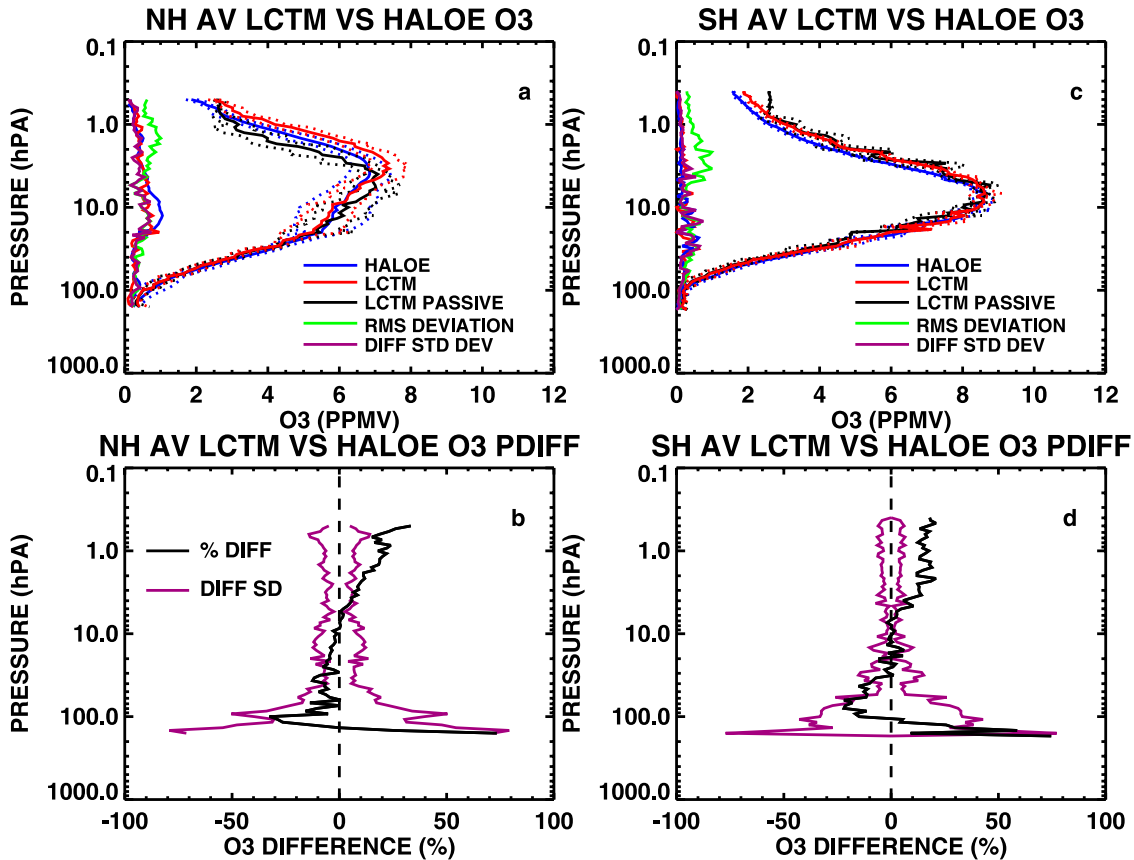


Figure 6. Northern and Southern Hemisphere coincident average profile comparisons of LCTM output with HALOE observations on 28 November 2004. The HALOE observations were not used in the LCTM initialization procedure. (a) Northern Hemisphere: Solid red profile is O_3 constructed from the average of all NH LCTM coincident values. Red dotted lines show $\pm 1\sigma$ variation. Red solid line with values less than 1 ppmv is 1σ standard deviation of LCTM O_3 . Black lines show LCTM output with passive advection. Blue lines show O_3 profile constructed from HALOE observations made on 28 November, which approximates a zonal mean at $\sim 45^\circ\text{N}$. Green and maroon profiles show RMS and difference standard deviations between the LCTM and HALOE values. The RMS difference is calculated as described in the caption to Figure 3. The difference standard deviation at a particular location is given by $\sigma = (\langle d^2 \rangle - \langle d \rangle^2)^{1/2}$, where d represents the set of coincident LCTM – HALOE differences $\{d_i\}$ at that location. (b) Percent difference between HALOE and LCTM coincident average profiles (black line), with difference standard deviation shown as percent of HALOE average profile O_3 values (maroon lines). (c) Same as Figure 6a except for the SH. (d) Same as Figure 6b, for SH.

the difference standard deviation (maroon line), and the RMS difference (green line), as explained in the figure caption. These indicate that variability of the LCTM/ HALOE differences is similar in magnitude to the zonal mean variability of the profiles, implying that the LCTM retains little longitudinal information from the HALOE initialization, as might be expected with 3-week trajectory lengths. Figure 6b shows the percent difference between the mean profiles, in addition to the standard deviation of the differences between coincident LCTM and HALOE data. Note that with the ~ 14 sunset or sunrise profiles HALOE makes during a single day, the standard error of the differences is a factor of 3–4 times smaller than the difference standard deviation shown in Figure 6b. Thus, in a statistical sense the percent difference between the mean profiles shown in Figure 6b (black line) is significant over much of the vertical range of the comparisons. It is also interesting to note whether the differences between the LCTM predictions and

the HALOE measurements are characterized by a relatively constant offset suggesting a model bias or are more or less random. In the former situation, the bias between the means will be relatively large, and the difference standard deviation will be relatively small. In the latter situation, this will be reversed.

[27] Figure 6b shows that biases between the mean profiles remain less than 20% between 1 and 100 hPa. Above ~ 5 hPa the LCTM is slightly high biased with the bias exceeding the difference standard deviation above ~ 3 hPa. This bias appears systematic, and could indicate small biases in the LCTM chemistry. Below ~ 10 hPa the LCTM is low biased by up to $\sim 10\%$. The difference standard deviation increases to greater than $\sim 30\%$ below ~ 80 hPa. These larger values in the lower stratosphere indicate increasingly large and random differences between the profiles, implying that the LCTM ability to predict subsequent HALOE measurements is decreasing.

[28] Figures 6c and 6d show that the SH behavior is similar to the NH. The SH profile shown in Figure 6c shows a 10–20% high bias in LCTM coincident O_3 above ~ 5 hPa, which exceeds the difference standard deviation. Active and passive run profiles shown in Figure 6c are very similar to each other, indicating that chemistry is not influencing the profile (though there is some influence of vertical smoothing via diffusion in the active profile). Below ~ 80 hPa in the SH, the RMS and standard deviation percent differences increase above $\sim 30\%$, indicating reduced model predictability. Figure 6 shows overall that LCTM predictions of O_3 are high biased by ~ 10 –20% above ~ 5 hPa, and suffer from increasing noise at altitudes below ~ 80 hPa. Within the range of ~ 80 –5 hPa, the LCTM can predict subsequent HALOE O_3 values to within $\sim 10\%$.

[29] Figure 7 is the same as Figure 6, except for CH_4 rather than O_3 . In both hemispheres, LCTM CH_4 agrees very well with the HALOE observations. The coincidence of active and passive LCTM profiles throughout the range indicates that chemical effects are small. There is a LCTM high bias of $\sim 10\%$ above ~ 5 hPa in the NH (Figure 7b). In the SH there are 20–30% high biases above ~ 2 hPa (Figure 7d). The largest RMS and standard deviation percent differences occur in the 1–10 hPa range, where there are large meridional CH_4 gradients. In contrast with the O_3 comparison, LCTM agreement with HALOE observations near 100 hPa is excellent, with virtually no bias and difference standard deviations $<10\%$.

[30] Profile plots of LCTM versus HALOE HCl are shown in Figure 8. Agreement between LCTM and HALOE

HCl is generally very good down to the lower stratosphere, and differences are small throughout the model vertical range. Again, the LCTM active and passive profiles show that the influence of chemistry is minimal. Similar to the case for O_3 , below ~ 80 –90 hPa, RMS and difference standard deviations become large, indicating reduced predictability at these pressure levels.

[31] Figure 9 compares LCTM and HALOE H_2O distributions. In the NH agreement is excellent. LCTM H_2O is virtually unbiased from below 100 hPa to above 1 hPa, with differences $< 5\%$. There is a constant $\sim 5\%$ low bias in the SH between 1 and 100 hPa. These differences are similar in magnitude to the difference standard deviations characterizing the SH profile.

[32] The figures above comparing HALOE-initialized LCTM output with subsequent HALOE observations show that the LCTM predicts subsequent measurements of HALOE O_3 , CH_4 , HCl, and H_2O generally to within $\sim 10\%$. In the case of O_3 and HCl, LCTM results appear to be valid above ~ 80 hPa, while the useful range for CH_4 and H_2O extend to below 100 hPa. Predictability for O_3 and CH_4 begins to degrade above ~ 5 hPa, while HCl and H_2O predictability extend above ~ 1 hPa. We obtain similar results to those presented above in the September 2004 and February 2005 time periods. These good comparisons suggest that the LCTM effectively propagates information from the HALOE observations used to initialize LCTM air parcels and effectively accounts for parcel chemical evolution and diffusion. This implies that the LCTM is a useful transfer standard for noncoincident evaluation of MLS

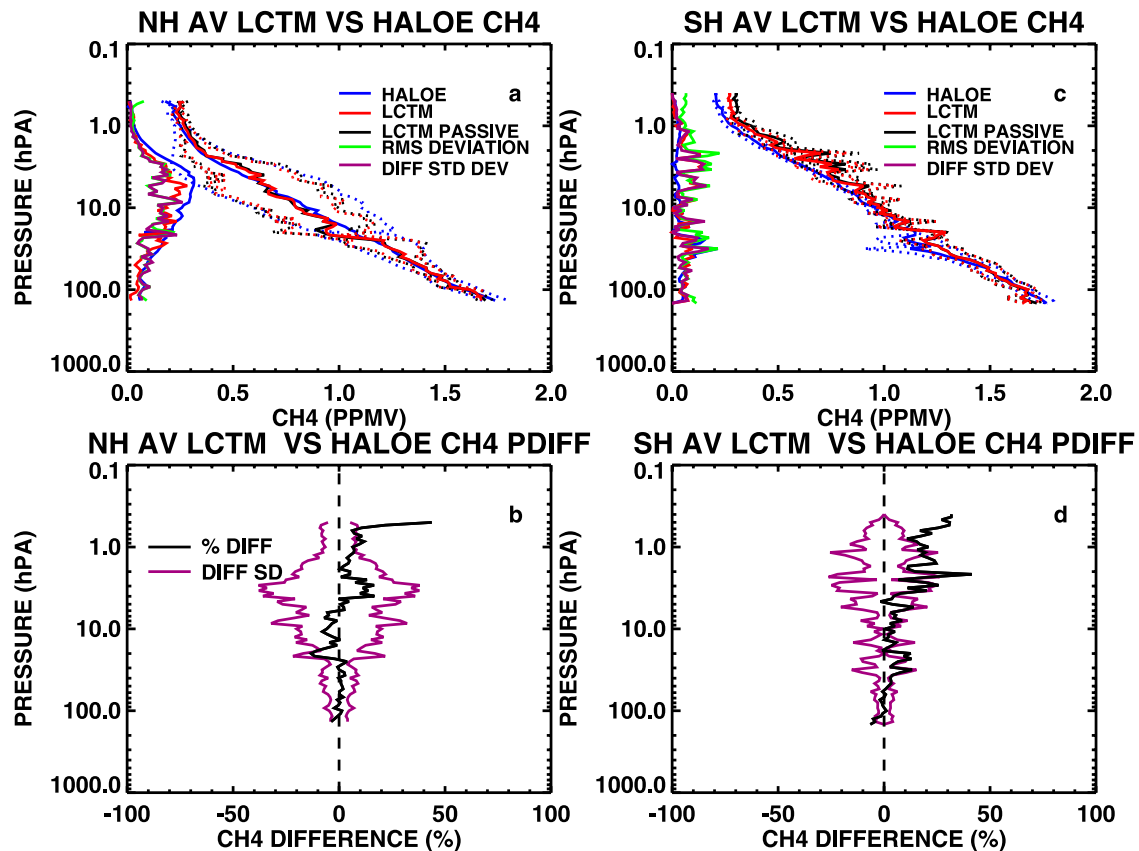


Figure 7. Same as Figure 6 except for CH_4 .

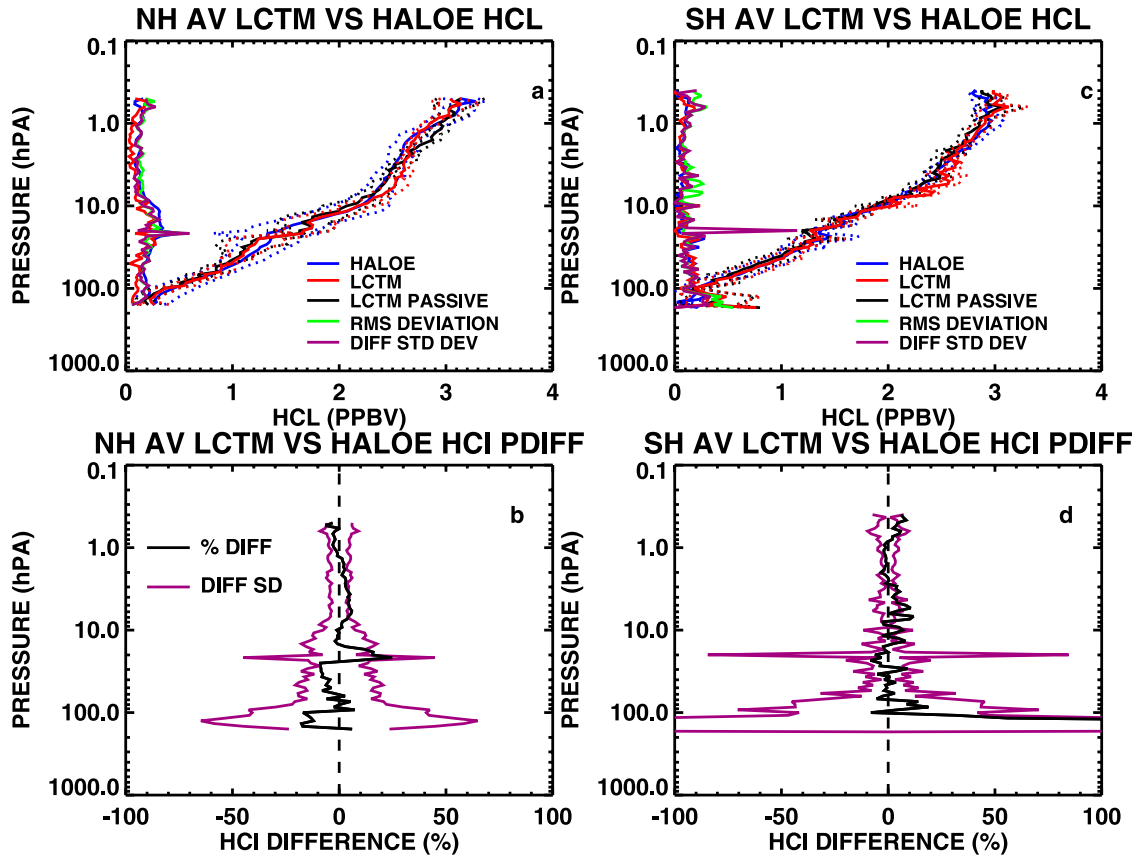


Figure 8. Same as Figure 6 except for HCl.

observations. In the next section, we examine LCTM/MLS comparisons.

6. Comparison to MLS Observations

[33] We now use the LCTM as a means of comparing noncoincident HALOE and MLS observations, by comparing MLS O₃, HCl, and H₂O observations with coincident, HALOE-initialized LCTM predictions. Version 2.2 observations are available on 17 September, 29 November, and 8 February, at the end of three 3-week periods having at least 14 d of HALOE observations available for LCTM initialization. Two other time periods exist (September and November 2005) in the HALOE/MLS overlap period which include both sufficient HALOE observations and v2.2 data. We do not examine these periods because of the consistency of our results in the three periods we have examined and present below.

[34] The method for generating coincident LCTM predictions is described in section 5, above, for comparing LCTM to HALOE observations. Here, we use narrower coincidence criteria of 5° longitude, 2° latitude, and 3 h. As with the HALOE comparisons shown in section 5 above, the coincidence criteria were determined from sensitivity studies, and our results do not depend critically on reasonable variations in the criteria.

[35] The MLS O₃ data were screened to eliminate poorly retrieved profiles by requiring that the Status flag not be an odd number, the Quality flag be >1.2, and the Convergence value <2.0. Precision values for each retrieved value were

required to be nonnegative. Figure 10 shows scatterplots of LCTM coincident predictions against MLS v2.2 O₃ observations made on 17 September 2004 (Figure 10, top), 29 November 2004 (Figure 10, middle), and 8 February 2004 (Figure 10, bottom). The plots consist respectively of ~15,000, ~20,000, or ~18,000 MLS measurements which could be matched with a coincident LCTM O₃ prediction on those days. Note that no area weighting was done, so some latitudes might be overrepresented in the figures. However, we did not notice strong latitude dependencies in the plots.

[36] Each point in Figure 10 is colored with the mean age of the LCTM parcels coincident with the MLS O₃ observation. The correlation between coincident LCTM predictions and MLS O₃ values is excellent on all three of the days, with a linear correlation coefficients of 0.97–0.98. The linear regression best fit slopes are all close to 1, indicating a nearly unbiased comparison. Older LCTM coincident values are nearly as well correlated as younger values. (Older coincident values tend to be slightly higher biased relative to the MLS value. However, the drift is much smaller than the variability of the agreement of same-age parcels with their corresponding MLS measurements.) Individual parcel uncertainties in the three panels are similar, ranging from 0.55 ppmv in September to 0.66 ppmv in February. This is 12–35% larger than the uncertainty for LCTM coincidences with subsequent HALOE observations shown in Figure 5a. When MLS O₃ values are around 1 ppmv, this constitutes an uncertainty of about 50–60%; at higher values, the uncertainty drops to a few percent of the MLS value.

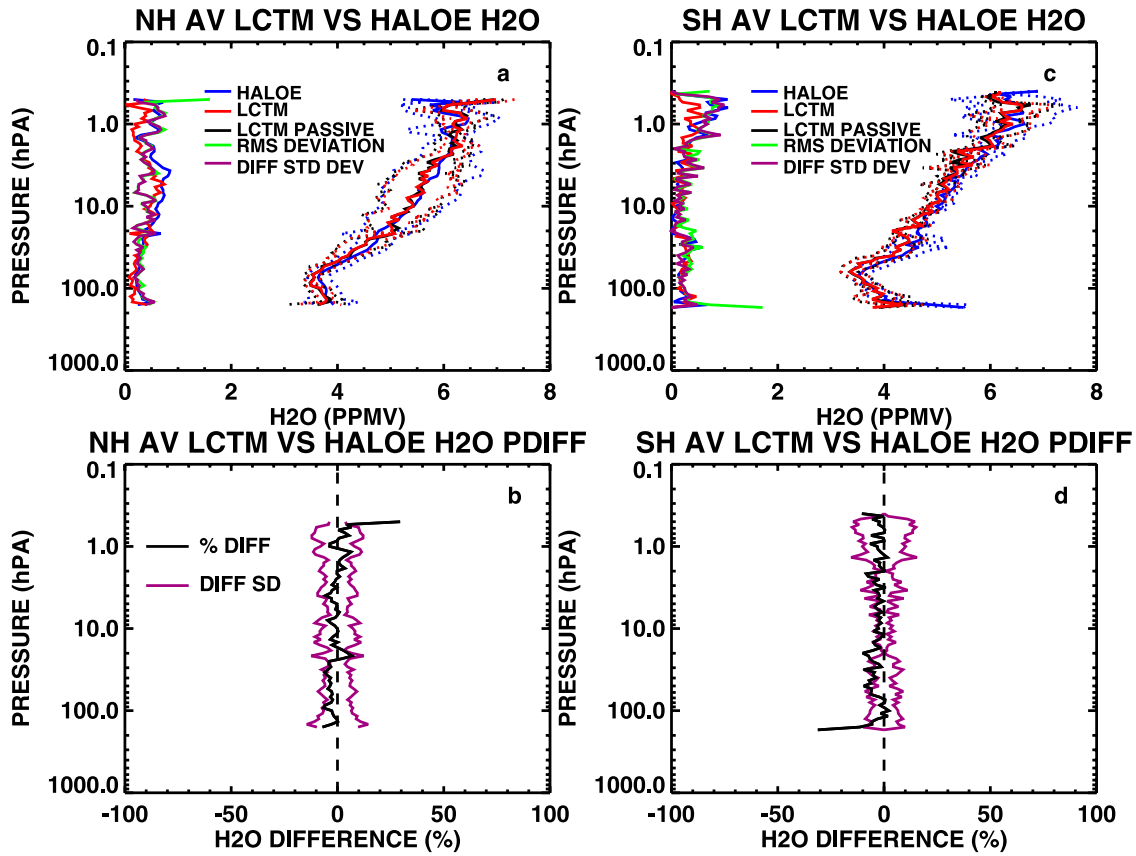


Figure 9. Same as Figure 6 except for H₂O.

[37] We now look at MLS HCl measurements. MLS v2.2 HCl data were filtered to include only measurements with an even Status flag, Quality >1.0, Convergence < 1.5, and positive precision. Figure 11 is the same as Figure 10, except for HCl. Only MLS values between 100 hPa and 0.2 hPa for which an LCTM coincidence could be identified are included in Figure 11. Points are color-coded by latitude. Figure 11 shows that LCTM and MLS HCl are well correlated, with correlation coefficients between 0.93–0.96. Above ~0.8 ppbv, the LCTM is low biased relative to MLS HCl, by as much as 25–30% at the highest HCl values. The color-coding by latitude shows that the highest MLS values of ~4 ppbv occur in the SH low to midlatitudes on 17 September, with larger contributions from the NH high latitudes on the other days. Figure 11 (top) also reveals a high bias of the LCTM relative to MLS for MLS values below ~0.5 ppbv, concentrated in the SH tropics and subtropics. The LCTM is also high biased relative to HALOE observations at this location, suggesting that model chemistry may be biasing the HCl results at this location and time. All three panels indicate consistent uncertainties for the LCTM predictions of 0.26–0.27 ppbv, ~60% larger than the uncertainty for LCTM coincidences with subsequent HALOE observations shown in Figure 5c.

[38] Figure 12 shows the correlation scatterplots of 17 September, 29 November, and 8 February for H₂O. MLS v2.2 H₂O measurements were filtered to exclude odd Status values, require Quality values greater than 0.9, and have positive precision. The points in Figure 12 are colored by potential temperature. The linear correlation

coefficients for H₂O are 0.89–0.90, worse than obtained for either O₃ or HCl. Uncertainties range from 0.44–0.53 ppmv, compared to the 0.41 ppmv uncertainty shown in Figure 5d. An obvious source of this reduced correlation in all three panels of Figure 12 is a secondary finger of MLS values ranging over 8 ppmv, which correspond to LCTM values between ~3 and 4 ppmv. Without this branch, the scatterplots would resemble those seen for HCl in Figure 12. Along the main branches, LCTM low biases reach ~25% at the highest H₂O values. Along the secondary branches, low biases can reach 50%.

[39] The points running along the secondary finger are generally at potential temperatures between 340–400 K, which places them in the upper troposphere/lower stratosphere region. It is also interesting to note that Figure 12 shows points at these potential temperatures where MLS is dry biased relative to LCTM values by over 25%. MLS H₂O values for these points are ~2–3 ppmv.

[40] To further explore the low-potential-temperature MLS H₂O concentrations, Figure 13 compares H₂O/O₃ scatterplots for coincident 29 November 2004 MLS observations (Figure 13, top) and LCTM predictions (Figure 13, bottom). The O₃ axis is plotted logarithmically to highlight the region below 1.0 ppmv, which corresponds to the lower stratosphere and upper troposphere. Between 0 and 1 ppmv, H₂O values were grouped into 0.1 ppmv O₃ bins. The black lines in Figure 13 show the bin mean values and ± 1 standard deviation lines. In the 0–1 ppmv O₃ range, the LCTM mean values range between 4% and 24% below the MLS mean values. The MLS H₂O data show more scatter than the

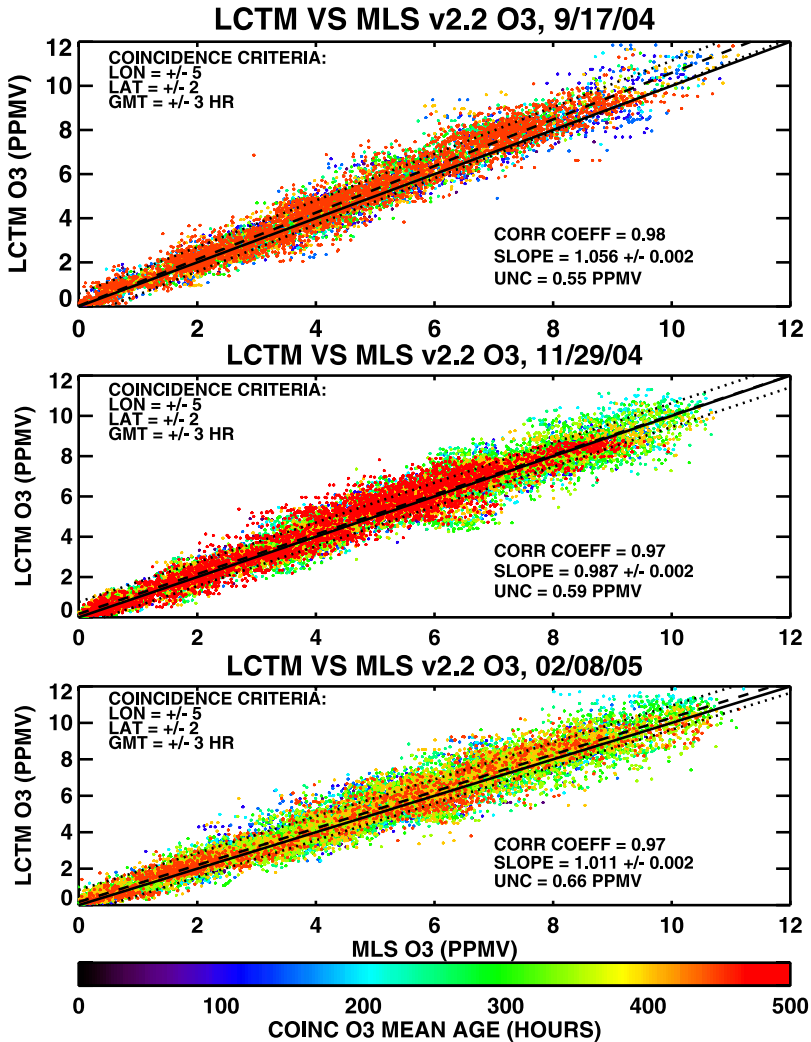


Figure 10. (top) Scatterplot of LCTM coincident O_3 values plotted against MLS O_3 observations made on 17 September 2004. Points are color-coded by the mean age of each LCTM coincident value. Solid line is the 1:1 correlation line. Dashed line is the linear regression best fit line. Dotted lines are the best fit line $\pm 1\sigma$ individual LCTM coincident value uncertainty. (middle) Scatterplot for 29 November 2004. (bottom) Scatterplot for 8 February 2005.

LCTM, with standard deviations ranging from $\sim 36\%$ in the 0–0.1 ppmv O_3 bin to $\sim 13\%$ in the 0.9–1 ppmv O_3 bin. This larger scatter at low O_3 mixing ratios of the MLS data accounts for the “finger” of high MLS values extending off the main axis in Figure 14, as well as the points showing MLS dry biased with respect to the LCTM.

[41] The scatterplots for O_3 , H_2O , and HCl presented above show good agreement between MLS and HALOE-initialized LCTM O_3 , and significant low biases of LCTM HCl and H_2O relative to MLS. The three different time periods examined demonstrate consistent results. A more detailed comparison is provided in Figure 14, which compares zonal mean profiles of O_3 , H_2O , and HCl generated from coincident data between 40°N and 50°N on 17 September, 29 November, and 8 February. In addition to MLS (blue) and LCTM (red) profiles, Figure 14 also shows profiles generated from passively advected HALOE observations; that is, no effects from LCTM chemistry or diffusion parameterizations are included. The O_3 profiles show good agreement between MLS and LCTM

profiles, though the LCTM is high biased at the peak on 17 September. Above the peak there are increasingly large differences between the profiles constructed from passively advected observations and the full LCTM profiles. The passively advected profiles do not agree as well with MLS, indicating the expected importance of chemical processes for O_3 at these altitudes. There are not large differences between passive and active LCTM profiles for HCl and H_2O . LCTM predictions are low biased for these species at all times. In the MLS H_2O profiles an oscillation is observed below 22 hPa. Between 100 and 200 hPa, the MLS profiles have substantially higher values than the LCTM profiles. This is discussed further below.

7. Comparison With MLS Zonal Means on 29 November

[42] The relatively high density of MLS observations and LCTM parcels makes it possible to compare zonal mean distributions. Figure 15 shows for the 29 November time

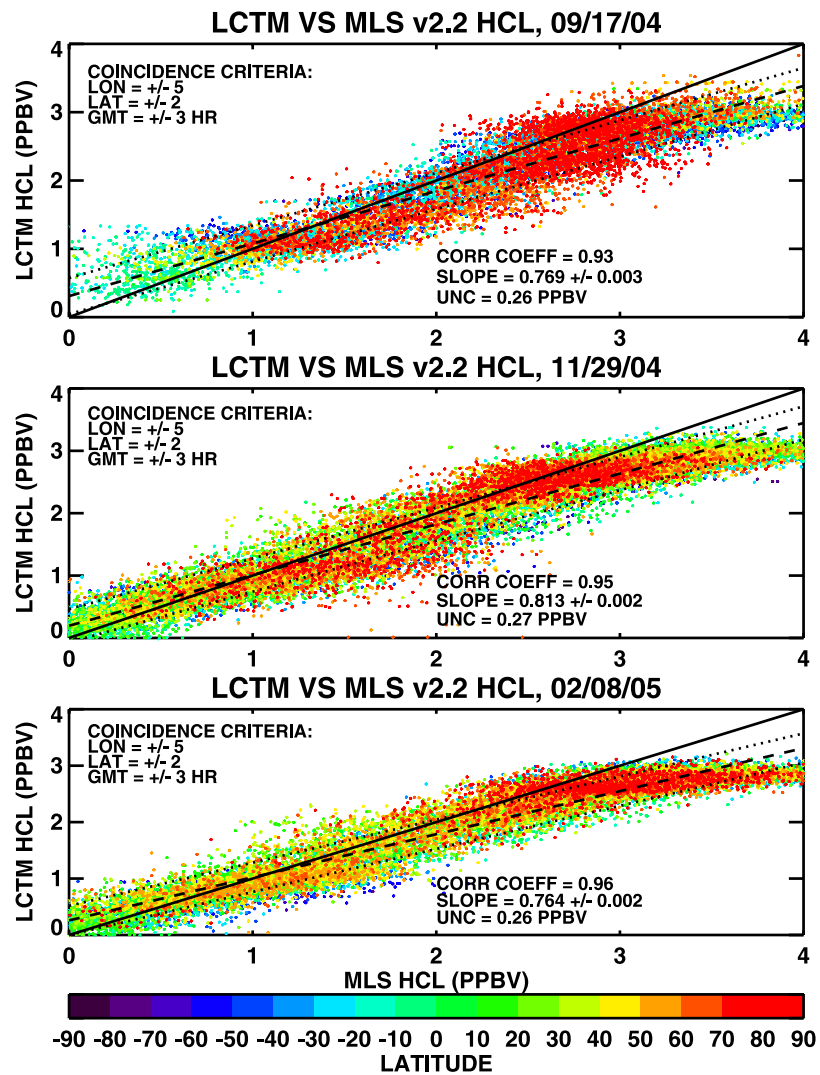


Figure 11. Same as Figure 10 except for HCl.

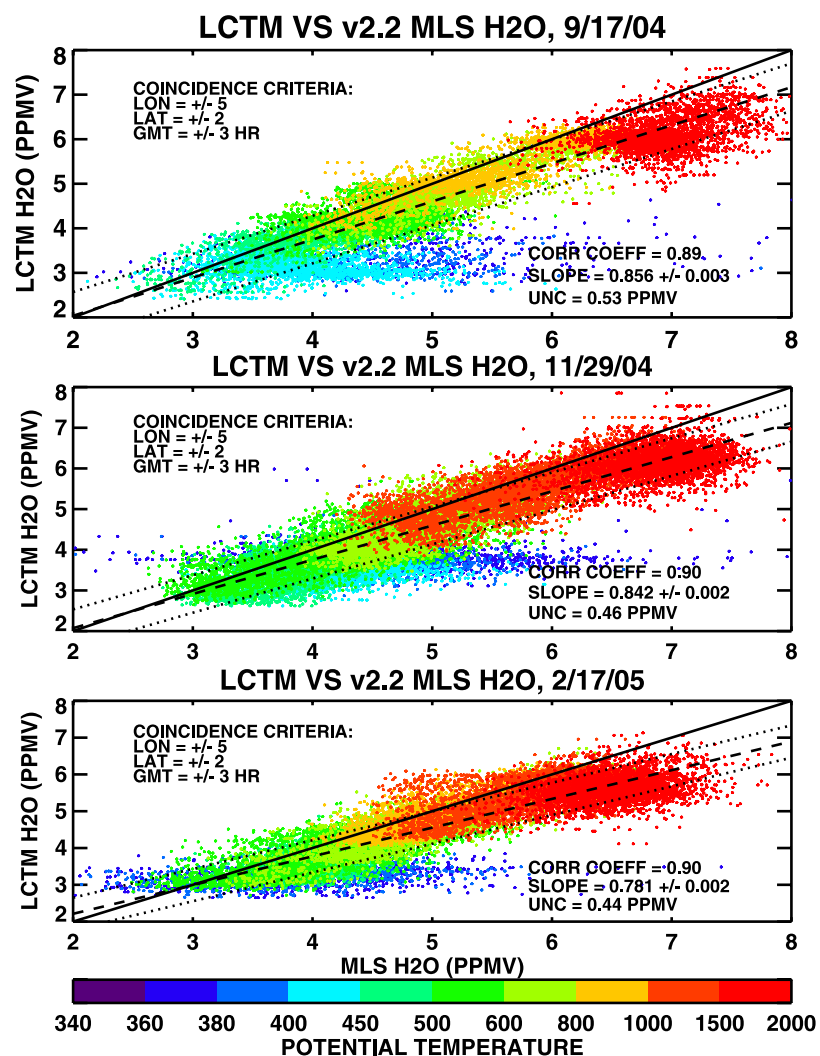


Figure 12. Same as Figure 10 except for H₂O.

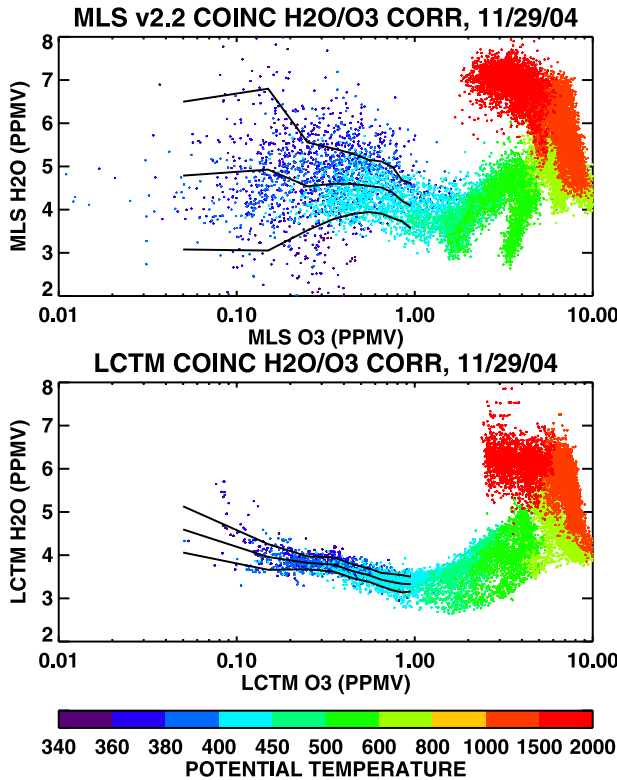


Figure 13. $\text{H}_2\text{O}/\text{O}_3$ scatterplot for (top) MLS and (bottom) LCTM. The black lines show mean H_2O values ± 1 standard deviation for 0.1-ppmv-wide O_3 bins for O_3 values ranging from 0 to 1 ppmv.

period the zonal mean distributions of MLS and coincident LCTM O_3 (Figure 15, top left and top right, respectively), the percent difference between the two distributions (Figure 15, bottom left), and the difference standard deviation between the two (Figure 15, bottom right). Because only the MLS values for which a coincident LCTM value could be calculated were used to generate the zonal mean figures, we refer to this type of figure as a “coincident zonal mean.” The meridional resolution of the plots is 10° , and vertical levels are the standard Aura pressure levels.

[43] Both of the coincident zonal mean plots shown in Figure 15 display the standard features of the stratospheric ozone distribution. The percent difference plot shown in Figure 15 reveals that LCTM/MLS O_3 differences are within 10% throughout much of the stratosphere, which as was discussed in section 5 above is about the predictability limit of the LCTM for O_3 . However, since there are generally ~ 60 – 80 points in each latitude/pressure bin, the standard error is $\sim 1/8$ of the difference standard deviation shown in the Figure 15 (bottom right), and the differences shown in Figure 15 (bottom left) are thus generally technically statistically significant. There is a tendency at all latitudes for LCTM O_3 to be slightly high biased near ~ 10 hPa, and low biased below this region, but these differences rarely exceed the difference standard deviation. (Locations where the absolute value of the difference exceeds the difference standard deviation are marked with asterisks.) The marked locations above 1 hPa should be ignored because the LCTM parcel density is low in this

region, and O_3 lifetimes are too short for much information from the HALOE initialization to be retained. The LCTM high bias south of 30°S between ~ 5 and 30 hPa can also be discounted. LCTM parcels there are the few that have moved rapidly from lower latitudes, where O_3 concentrations are higher. These parcels cannot be considered representative of the SH middle to high latitudes near the end of spring, a region influenced by the effects of Antarctic ozone depletion. In the tropics, the difference plot in Figure 11 shows a dipolar structure marked by asterisks where the LCTM is $> 10\%$ high biased at ~ 5 hPa, and low biased at ~ 20 hPa. This dipolar structure straddles the 10 hPa O_3 peak, and is possibly a signature of too-rapid tropical upwelling. (The GEOS-4 DAS is known to have a somewhat over-vigorous circulation [Pawson et al., 2007].) The marked LCTM high bias in the tropical UT/LS region is the result of very rapid equatorial transport of O_3 between 100 and 200 hPa in both the NH and SH. Thus, these differences again do not suggest any problems with the MLS O_3 retrieval.

[44] Froidevaux et al. [2006] compared Aura v1.5 MLS O_3 with HALOE O_3 measurements using coincident validation. They found a very close agreement of $\sim 5\%$ between 3-month, globally averaged profiles constructed from the data extending between 100 and 1 hPa. Our results show that this close agreement between the two measurements also holds for daily MLS O_3 measurements on 29 November, at latitudes between $\sim 40^\circ\text{S}$ and 90°N , outside of the NH polar vortex, between ~ 100 and 1 hPa, for version 2.2 O_3 data.

[45] Figure 16 shows the coincident zonal mean figure for HCl, similar to Figure 15. The morphology of the MLS and LCTM coincident zonal mean plots are similar. The primary difference between the MLS and LCTM coincident zonal mean plots shown in the top left and right panels of Figure 16, respectively, is that the LCTM is low biased relative to MLS. The bottom left panel of Figure 16 shows this low bias of ~ 15 – 30% , which exceeds difference standard deviations throughout much of the stratosphere. The low bias in the SH is larger than in the NH. The LCTM is high biased in the tropical lower stratosphere, with wings extending out to midlatitudes near 100 hPa, but these biases are hard to interpret given the difference standard deviations shown in Figure 16 (bottom right).

[46] Russell et al. [1996] found 8–19% low biases of HALOE HCl with respect to balloon profiles, and 10–20% low biases in comparison to Atmospheric Trace Molecule Spectroscopy (ATMOS) instrument profiles made from the space shuttle [Raper et al., 1987; Zander et al., 1990, 1992]. Liu et al. [1996] also found profiles retrieved from ground-based measurements near Denver, Colorado, to be high biased by 5–20% relative to HALOE HCl between 20 and 42 km. These low biases, which are within the combined uncertainties of the measurements, are similar to the biases we have found between the MLS HCl data and HALOE-initialized LCTM predictions. The comparisons shown in Figure 16 are also broadly consistent with the results of the Froidevaux et al. [2006] coincident comparison of HALOE and MLS HCl.

[47] Figure 17 shows coincident zonal mean plots for MLS and LCTM H_2O , the percent difference between the two, and the difference standard deviation. The LCTM

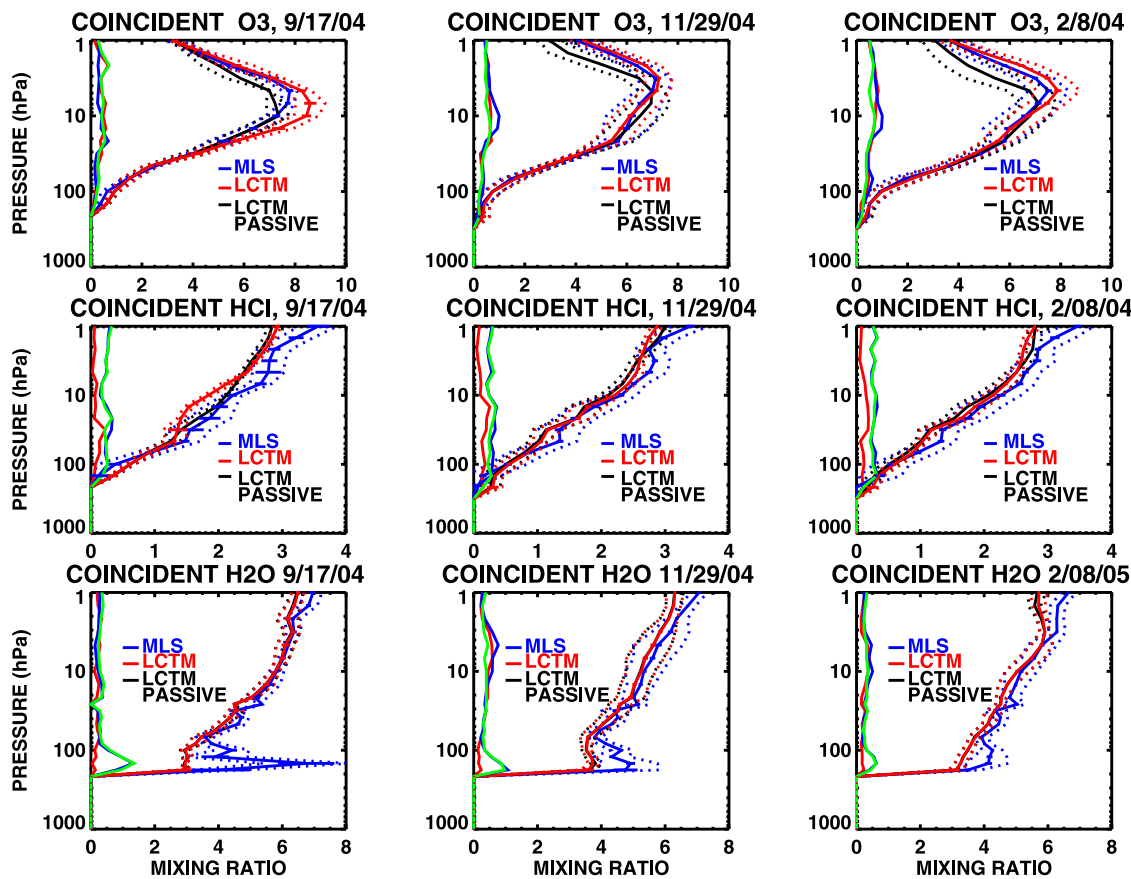


Figure 14. Zonal mean profiles for MLS (blue lines), LCTM (red lines) and passive LCTM (black lines), constructed from coincident parcels between 40°N and 50°N. Uncertainty bounds are dotted lines. Green line is the difference standard deviation profile. Solid blue and red lines near difference standard deviation are profile standard deviations for MLS (blue) and LCTM (red).

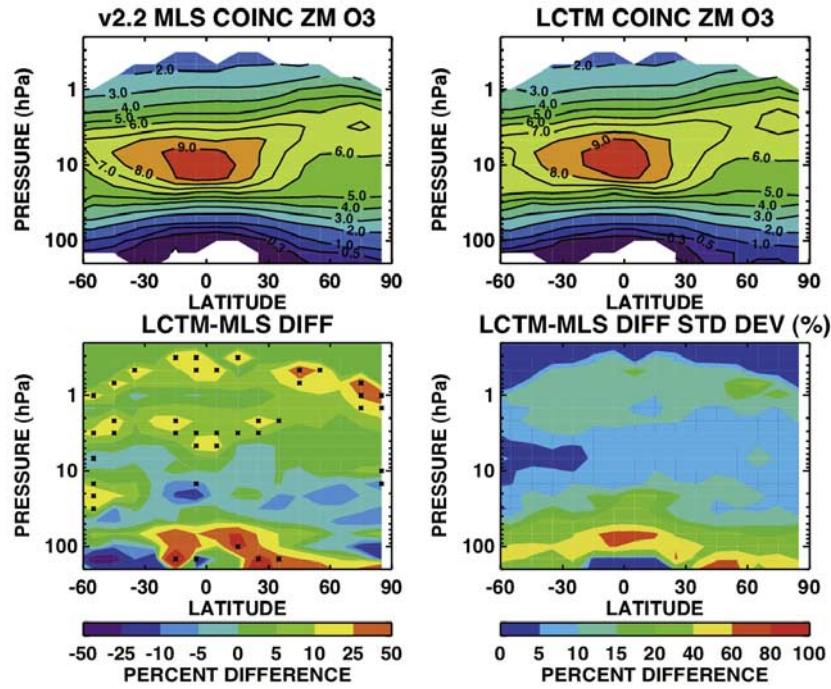


Figure 15. Coincident zonal mean comparisons of MLS and LCTM O₃ for 29 November 2004. (top left) Zonal mean constructed from MLS observations for which a coincident LCTM value exists. Horizontal resolution is 10°, and vertical levels are standard Aura pressure levels. (top right) Zonal mean constructed from coincident LCTM values. (bottom left) Percent difference between the LCTM and MLS coincident zonal means. Locations where the percent difference magnitude exceeds the difference standard deviation are marked by asterisks. (bottom right) Difference standard deviation between the MLS and LCTM coincident zonal mean distributions.

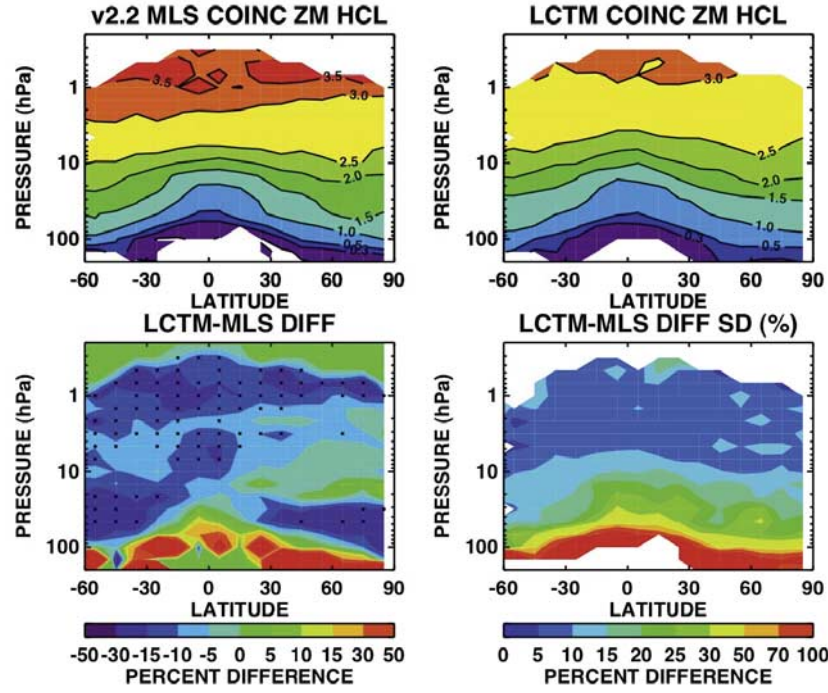


Figure 16. Same as Figure 15 except for HCl.

coincident zonal mean is similar in morphology to the MLS plot, but the MLS plot is not as smooth and exhibits vertical oscillations in the lower stratosphere at altitudes below ~ 20 hPa, as was seen in Figure 14. If such vertical oscillations occurred in the HALOE data used to initialize the LCTM, the vertical diffusivity of the model over the 3-week trajectory time period is insufficient to smooth them out. Thus the vertical oscillations appear to be MLS retrieval artifacts. There is a particularly large oscillation between the 26 and 32 hPa levels, with the 26 hPa level high biased relative to the 32 hPa level. The percent difference shown in Figure 17 (bottom left) ranges from a small low bias of between 5 and 10% near 10 hPa to up to 30% low biases in the upper stratosphere and 30–50% low biases in the lower stratosphere/upper troposphere NH and SH midlatitudes.

[48] Version 19 HALOE H_2O is known to be low biased relative to coincident measurements [Kley *et al.*, 2000]. At higher H_2O values this low bias of $\sim 10\text{--}20\%$ is due to detector nonlinearity effects which are not accounted for in the retrieval. In the lower stratosphere, the O_2 continuum is an interfering absorber in the H_2O channel. The temperature dependence of this interference is not treated completely in version 19 HALOE retrievals. Biases here are $\sim 20\%$. The known low biases in HALOE H_2O can account for some of the discrepancy between MLS and LCTM distributions in the lower stratosphere. In the upper troposphere at latitudes near $\pm 30^\circ$, where the low bias is $\sim 50\%$, the LCTM may be low because of small parcel densities and possible sampling biases since the parcels have been transported rapidly from higher latitudes and altitudes. The vertical oscillations and broader precision limits of the MLS data may also contribute to the discrepancies here.

[49] The lower stratospheric vertical oscillations seen in the MLS data have been discussed in the MLS v1.5 data quality document. These artifacts are still present in the v2.2 retrieval, though they have been reduced significantly from the v1.5 and v2.10 data. They are still under investigation at this time, but one possibility is that they are due to an instrument effect which has not been accounted for in the level 1 radiances. As is the case with O_3 and HCl above, the MLS/LCTM H_2O comparisons shown here are generally consistent with differences between HALOE and MLS H_2O shown by Froidevaux *et al.* [2006].

8. Summary and Conclusions

[50] We have used the Langley LCTM to intercompare asynchronous v19 HALOE measurements of HCl, H_2O , and O_3 with v2.2 Aura MLS measurements on 17 September 2004, 29 November 2004, and 8 February 2005. HALOE measurements made during the 3 weeks previous to each of these dates were used to initialize air parcels in the LCTM, which were then propagated forward in time, subjected to advective transport, photochemistry and diffusion.

[51] The capability of the LCTM to predict the photochemical evolution of the atmosphere was tested by comparing LCTM output with later HALOE measurements of O_3 , CH_4 , HCl and H_2O . The LCTM/HALOE comparisons were characterized by small biases, relatively low uncertainties, and high linear correlation coefficients. Zonal mean profiles constructed from LCTM output matched subsequent HALOE H_2O and CH_4 profiles to within $\sim 5\text{--}10\%$ between 100 and 1 hPa, and O_3 and HCl profiles to $\sim 10\%$ between 80 and 5 hPa.

[52] Comparisons of LCTM predictions and MLS observations show similar results for all three time periods

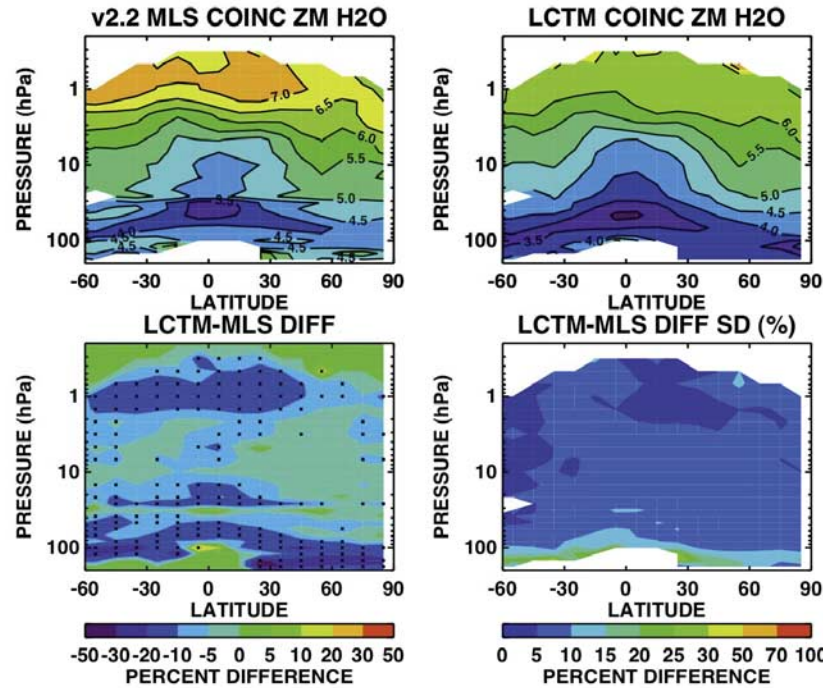


Figure 17. Same as Figure 15 except for H₂O.

examined. MLS O₃ observations show very good agreement with coincident LCTM predictions from the Northern Hemisphere high latitudes into the Southern Hemisphere midlatitudes. Differences are generally < 10%. The LCTM HCl distribution is low biased with respect to MLS by up to ~25% in the upper stratosphere. There are also discrepancies between LCTM predictions and MLS observations for H₂O. In the middle to upper stratosphere, LCTM predictions are low biased by up to 15%. In the lower stratosphere/upper troposphere region, low biases range from 30 to 50%. In addition, the LCTM shows no evidence of the oscillations at alternate levels seen in MLS measurements made in the tropical to midlatitude lower stratosphere.

[53] These differences are generally consistent with results obtained by *Froidevaux et al.* [2006], using a coincident validation technique. Our study complements these coincident comparisons, and suggests that the paper's conclusions regarding the differences between HALOE and MLS observations of O₃, HCl, and H₂O, which were based on seasonal and hemispheric averages, also appear to hold at daily temporal and zonal spatial scales.

[54] **Acknowledgments.** We would like to thank E. E. Remsberg (NASA Langley Research Center), G. A. Morris (Valparaiso University), W. G. Read (Jet Propulsion Laboratory), and H. Vömel (University of Colorado) for helpful discussions. Work at the Jet Propulsion Laboratory, California Institute of Technology, was carried out under a contract with NASA. We would also like to thank the rest of the MLS science team for their efforts in creating the MLS data set. This work was funded by the NASA Aura validation program (P. DeCola, program manager).

References

- Al-Saadi, J. A., R. B. Pierce, M. Natarajan, T. D. Fairlie, and W. L. Grose (2004), Chemical climatology of the middle atmosphere simulated by the NASA Langley Research Center Interactive Modeling Project for Atmospheric Chemistry and Transport (IMPACT) model, *J. Geophys. Res.*, *109*, D17301, doi:10.1029/2003JD004354.
- Bloom, S., et al. (2005), Documentation and validation of the Goddard Earth Observing System (GEOS) data assimilation system—Version 4,
- Technical Report Series on Global Modeling and Data Assimilation, NASA/TM-2005-104606, vol. 26.
- Brühl, C., et al. (1996), Halogen Occultation Experiment ozone channel validation, *J. Geophys. Res.*, *101*, 10,217–10,240, doi:10.1029/95JD02031.
- Danilin, M. Y., et al. (2002), Trajectory hunting as an effective technique to validate multiplatform measurements: Analysis of the MLS, HALOE, SAGE-II, ILAS, and POAM-II data in October–November 1996, *J. Geophys. Res.*, *107*(D20), 4420, doi:10.1029/2001JD002012.
- Fahey, D. W., et al. (2001), The detection of large HNO₃-containing particles in the winter Arctic stratosphere, *Science*, *291*, 1026–1031, doi:10.1126/science.1057265.
- Fairlie, T. D., R. B. Pierce, J. A. Al-Saadi, W. L. Grose, J. M. Russell III, M. H. Proffitt, and C. Webster (1999), The contribution of mixing in Lagrangian photochemical predictions of polar ozone loss over the Arctic in summer 1997, *J. Geophys. Res.*, *104*, 26,597–26,609, doi:10.1029/1999JD900111.
- Froidevaux, L., et al. (2006), Early validation analyses of atmospheric profiles from EOS MLS on the Aura satellite, *IEEE Trans. Geosci. Remote Sens.*, *44*, 1106–1121, doi:10.1109/TGRS.2006.864366.
- Harries, J. E., J. M. Russell III, A. F. Tuck, L. L. Gordley, P. Purcell, K. Stone, R. M. Bevilacqua, M. Gunson, G. Nedoluha, and W. A. Traub (1996), Validation of measurements of water vapor from the Halogen Occultation Experiment (HALOE), *J. Geophys. Res.*, *101*, 10205–10216, doi:10.1029/95JD02933.
- Kley, D., J. M. Russell III, and C. Phillips (Eds.) (2000), SPARC assessment of upper tropospheric and stratospheric water vapor, *Tech. Rep. WCRP 113, WMO/TD 1043*, SPARC, Paris.
- Lait, L. R., et al. (2004), Non-coincident inter-instrument comparisons of ozone measurements using quasi-conservative coordinates, *Atmos. Chem. Phys.*, *4*, 2345–2352.
- Liu, X., F. J. Murcay, and D. G. Murcay (1996), Comparison of HF and HCl vertical profiles from ground-based high-resolution infrared solar spectra with Halogen Occultation Experiment observations, *J. Geophys. Res.*, *101*(D6), 10175–10181.
- Livesey, N. J., et al. (2005), Version 1.5 level 2 data quality and description document, *JPL D-32381*, Jet Propul. Lab., Pasadena, Calif.
- Morris, G. A., J. F. Gleason, J. M. Russell III, M. R. Schoeberl, and M. P. McCormick (2002), A comparison of HALOE V19 with SAGE II V 6.00 ozone observations using trajectory mapping, *J. Geophys. Res.*, *107*(D13), 4177, doi:10.1029/2001JD000847.
- Park, J. H., et al. (1996), Validation of Halogen Occultation Experiment CH₄ measurements from UARS, *J. Geophys. Res.*, *101*, 10,183–10,203, doi:10.1029/95JD02736.
- Pawson, S., I. Stanjek, S. R. Kawa, H. Hayasi, W.-W. Tan, J. E. Nielsen, Z. Zhu, L.-P. Chang, and N. J. Livesey (2007), Stratospheric transport

- using 6-h-averaged winds from a data assimilation system, *J. Geophys. Res.*, *112*, D23103, doi:10.1029/2006JD007673.
- Pierce, R. B., J. A. Al-Saadi, T. D. Fairlie, J. R. Olson, R. S. Eckman, W. L. Grose, G. S. Lingenfelser, and J. M. Russell (1999), Large-scale stratospheric ozone photochemistry and transport during the POLARIS Campaign, *J. Geophys. Res.*, *104*(D21), 26525–26545, doi:10.1029/1999JD900395.
- Pierce, R. B., et al. (2003), Large-scale chemical evolution of the Arctic vortex during the 1999/2000 winter: HALOE/POAM III Lagrangian photochemical modeling for the SAGE III-Ozone Loss and Validation Experiment (SOLVE) campaign, *J. Geophys. Res.*, *108*(D5), 8317, doi:10.1029/2001JD001063.
- Raper, O. F., C. B. Farmer, R. Zaner, and J. H. Park (1987), Infrared spectroscopic measurements of halogenated sink and reservoir gases in the stratosphere with the ATMOS instrument, *J. Geophys. Res.*, *92*, 9851–9858, doi:10.1029/JD092iD08p09851.
- Russell, J. M., III, L. L. Gordley, J. H. Park, S. R. Drayson, W. D. Hesketh, R. J. Cicerone, A. F. Tuck, J. E. Frederick, J. E. Harries, and P. J. Crutzen (1993), The Halogen Occultation Experiment, *J. Geophys. Res.*, *98*, 10777–10798, doi:10.1029/93JD00799.
- Russell, J. M., III, et al. (1996), Validation of hydrogen chloride measurements made by the Halogen Occultation Experiment from the UARS platform, *J. Geophys. Res.*, *101*, 10151–10162, doi:10.1029/95JD01696.
- Sander, S. P., et al. (2006), Chemical kinetics and photochemical data for use in atmospheric studies, evaluation number 15, *JPL Publ. 06-2*, Jet Propul. Lab., Pasadena, Calif.
- Zander, R., M. R. Gunson, J. C. Foster, C. P. Rinsland, and J. Namkung (1990), Stratospheric ClONO₂, HCl, and HF concentration profiles derived from atmospheric trace molecule spectroscopy experiment Spacelab 3 observations: An update, *J. Geophys. Res.*, *95*, 20,519–20,525, doi:10.1029/905iD12p20519.
- Zander, R., M. R. Gunson, C. B. Farmer, C. P. Rinsland, F. W. Irion, and E. Mahieu (1992), The 1985 chlorine and fluorine inventories in the stratosphere based on ATMOS observations at 30° north latitude, *J. Atmos. Chem.*, *15*, 171–186, doi:10.1007/BF00053758.
-
- D. B. Considine, T. D. Fairlie, M. Natarajan, and R. B. Pierce, NASA Langley Research Center, Hampton, VA 23681, USA. (david.b.considine@nasa.gov)
- L. Froidevaux and A. Lambert, Jet Propulsion Laboratory, California Institute of Technology, Pasadena, CA 91109, USA.
- G. S. Lingenfelser, Science Systems and Applications International, Inc., Hampton, VA 23681, USA.